

## PHASE DIAGRAMS IN NONLOCAL POLYAKOV–NAMBU–JONA-LASINIO MODELS CONSTRAINED BY LATTICE QCD RESULTS

G. A. Contrera <sup>a, b, c</sup>, A. G. Grunfeld <sup>b, d</sup>, D. B. Blaschke <sup>c, e</sup>

<sup>a</sup> Gravitation, Astrophysics and Cosmology Group, FCAyG, UNLP, La Plata, Argentina

<sup>b</sup> CONICET, Buenos Aires, Argentina

<sup>c</sup> Institute for Theoretical Physics, University of Wroclaw, Wroclaw, Poland

<sup>d</sup> Departamento de Física, Comisión Nacional de Energía Atómica, Buenos Aires, Argentina

<sup>e</sup> Joint Institute for Nuclear Research, Dubna

Based on lattice QCD-adjusted  $SU(2)_f$  nonlocal Polyakov–Nambu–Jona-Lasinio (PNJL) models, we investigate *how* the location of the critical endpoint in the QCD phase diagram depends on the strength of the vector meson coupling, as well as on the Polyakov-loop (PL) potential and the form factors of the covariant model. The latter are constrained by lattice QCD data for the quark propagator. The strength of the vector coupling is adjusted so as to reproduce the slope of the pseudocritical temperature for the chiral phase transition at low chemical potential extracted recently from lattice QCD simulations. Our study supports the existence of a critical endpoint in the QCD phase diagram albeit the constraint for the vector coupling shifts its location to lower temperatures and higher baryochemical potentials than in the case without it.

На основе нелокальной модели Намбу–Йона–Лазинио с петлей Полякова, обусловленной данными  $SU_f(2)$  КХД на решетке, мы изучили, как положение критической точки фазовой диаграммы КХД зависит от константы векторной связи, а также от потенциала петли Полякова и формфакторов ковариантного взаимодействия модели. Все это определяется данными, полученными для кваркового пропагатора в решеточной КХД. Константа векторной связи определяется воспроизведением данных, полученных на решетке для наклона псевдокритической температуры кирального фазового перехода в области низких химических потенциалов. Наше исследование подтверждает существование критической точки на фазовой диаграмме, однако в присутствии векторной связи ее положение определяется при более низкой температуре и более высоком химическом потенциале барионного заряда, чем без нее.

PACS: 05.70.Jk; 11.10.Wx; 11.30.Rd; 12.38.Mh; 12.39.Ki; 25.75.Nq

### INTRODUCTION

The QCD phase diagram has been focus of intense research in the last decades. The conjecture for the existence of a critical endpoint (CEP) of first-order phase transitions in the QCD phase diagram is the basis for recent as well as future beam energy scan (BES) programs in relativistic heavy-ion collision experiments at RHIC, SPS, NICA and FAIR which try to

identify the parameters of its position ( $T_{\text{CEP}}, \mu_{\text{CEP}}$ ). The theoretical situation is very unsatisfactory since the predictions for this position form merely a skymap in the  $T-\mu$  plane [1]. Quantitative calculations of the phase diagram based in QCD are extremely complicated in the low energy regime due to its strong coupling. In this region nonperturbative methods are powerful tools to describe the chiral and deconfinement transitions. Lattice QCD calculations have the sign problem at finite chemical potential. Therefore, the effective models play a crucial role to describe the phase diagram, especially at finite densities.

The now well-established results from lattice QCD at zero and small chemical potential  $\mu$  predict coincident chiral and deconfinement crossover transitions at a pseudocritical temperature of  $T_c(0) = (154 \pm 9)$  MeV for 2 + 1 flavors [2] and a value of  $T_c(0) \sim 170$  MeV for two flavors [3].

A possible strategy for extending these benchmark results to the so far inaccessible regions of the QCD phase diagram is to use effective theories for the low-energy sector of QCD, which reproduce lattice results at vanishing and small  $\mu$ , and systematically extend the predictions to high chemical potential without changing the model inputs fixed with lattice results for the QCD vacuum. That leaves us with a variety of possibilities for the phase structure at nonzero  $\mu$ , depending on the effective model.

Among them we want to mention the following ones:

- no CEP at all [4], since the transition is crossover in the whole phase diagram;
- no CEP, but a Lifshitz point [5];
- one CEP, but with largely differing predictions of its position [1];
- second CEP [6–9];
- several CEPs [10, 11];
- CEP and triple point, possibly coincident, due to another phase (i.e., color superconducting [12] or quarkyonic matter [13]) at low temperatures and high densities.

This spectrum of possibilities is rather broad in view of the upcoming experimental programmes. It is crucial to analyze the predictions arising from effective models for their compatibility with lattice results.

One of the effective models that accounts for dynamical breaking of chiral symmetry and its restoration at finite  $T$  and  $\mu$  is the Nambu–Jona-Lasinio (NJL) model [14–17]. The absence of confinement in this model is partially cured by coupling its chiral quark sector to the Polyakov-loop variable and adjusting a suitable potential with a temperature dependence that is adjusted to describe the pressure in accordance with lattice QCD simulations in the pure gauge field system [18–20]. These PNJL models provide a straightforward approach to the behavior of chiral and Polyakov-loop order parameters in the  $T-\mu$  plane (the phase diagram, see also [21, 22]) and predict a position for the CEP.

It has been shown that the nonlocal version of the PNJL model reproduces hadron properties at zero density and temperature, and presents some advantages over the local model [23–25]. As another feature, one can add to the model a vector repulsive interaction which increases the stiffness of quark matter and is therefore indispensable to discuss, under the observational constraint of  $2 M_\odot$  neutron stars [26, 27], the possibility of quark matter phases in their interiors [28–32]. Such astrophysical applications have recently also been considered within the nonlocal PNJL model [33–36].

Our aim in the present paper is to make a systematic study of the location of the CEP based on chiral quark models constrained from lattice results, including all interactions mentioned

above. We tune the parameters of our model to reproduce lattice results at zero density and then we extrapolate our predictions to regions of finite density or chemical potential.

This article is organized as follows. In Sec. 1 we present the description of the model and the parametrizations we used. In Sec. 2 we show our results for the different form factors and parameters. Then, in Sec. 3 we present our conclusions.

## 1. GENERAL FORMALISM

Let us start describing the general formalism of the model we used. In the present work we considered a nonlocal  $SU(2)_f$  chiral model, including vector interactions as well as quark couplings to the gauge color background fields.

**1.1. Nonlocal Chiral Quark Model.** The corresponding Lagrangian of the model used in this work is given by

$$\mathcal{L} = \bar{q}(i\cancel{D} - m_0)q + \mathcal{L}_{\text{int}} + \mathcal{U}(\Phi), \quad (1)$$

where  $q$  is the  $N_f = 2$  fermion doublet  $q \equiv (u, d)^T$ , and  $m_0$  is the current quark mass (we consider isospin symmetry, that is  $m_0 = m_u = m_d$ ). The covariant derivative is defined as  $D_\mu \equiv \partial_\mu - iA_\mu$ , where  $A_\mu$  are color gauge fields.

The nonlocal interaction channels are given by

$$\mathcal{L}_{\text{int}} = -\frac{G_S}{2} [j_a(x)j_a(x) - j_P(x)j_P(x)] - \frac{G_V}{2} j_V(x)j_V(x), \quad (2)$$

where the nonlocal currents are

$$\begin{aligned} j_a(x) &= \int d^4z g(z) \bar{q}\left(x + \frac{z}{2}\right) \Gamma_a q\left(x - \frac{z}{2}\right), \\ j_P(x) &= \int d^4z f(z) \bar{q}\left(x + \frac{z}{2}\right) \frac{i\cancel{\partial}}{2\kappa_p} q\left(x - \frac{z}{2}\right), \\ j_V(x) &= \int d^4z g(z) \bar{q}\left(x + \frac{z}{2}\right) \gamma^0 q\left(x - \frac{z}{2}\right), \end{aligned} \quad (3)$$

with  $\Gamma_a = (\Gamma_S, \Gamma_P) = (\mathbb{1}, i\gamma_5 \vec{\tau})$  for scalar and pseudoscalar currents, respectively, and  $u(x') \overset{\leftrightarrow}{\partial} v(x) = u(x') \partial_x v(x) - \partial_{x'} u(x') v(x)$ . The functions  $g(z)$  and  $f(z)$  are nonlocal covariant form factors. The scalar-isoscalar component of the  $j_a(x)$  current is the responsible for the momentum dependence of the quark mass in the quark propagator. Then, the current  $j_P(x)$  will generate a momentum-dependent wave function renormalization (WFR) of this propagator. The mass parameter  $\kappa_p$  controls the relative strength between both interaction terms in (3). Finally,  $j_V(x)$  represents the vector channel interaction current, whose coupling constant  $G_V$  is usually taken as a free parameter. Moreover, we also have considered in this vector interaction the same nonlocal covariant form factor  $g(z)$  used for the scalar and pseudoscalar currents. Then it is not necessary to include new free parameter in this term.

After the Fourier transform into momentum space, we have performed a standard bosonization of the theory introducing the bosonic fields  $\sigma_{1,2}(p)$  and  $\omega(p)$ , and integrate out the quark fields. Furthermore, as we work within the mean field approximation (MFA), we replace the bosonic fields by their vacuum expectation values  $\sigma_{1,2}$  and  $\omega$ , respectively, and the corresponding fluctuations are neglected. The main motivation of the present work is to study the

phase diagram of the strongly interacting quark matter. As we want to analyze the chiral phase transition for different choices of the parameters of the model, we have to include the dependence on the temperature  $T$  and quark chemical potential  $\mu$  in our effective action<sup>1</sup>. In the present work this is carried out by using the Matsubara imaginary time formalism. As mentioned above, the quarks are coupled to the gluons in (1) through the covariant derivative.

The coupling of fermions with the gluon fields is taken into account in (1) through the covariant derivative. Considering the quarks in a color field background  $A_0 = g_0 G_\mu^a \lambda_a / 2$ , where  $G_\mu^a$  are the  $SU(3)$  color gauge fields. At mean field level the traced Polyakov loop is given by  $\Phi = \frac{1}{3} \text{Tr} \exp(i\beta\phi)$ , with  $\phi = i\bar{A}_0$ . Then, in the Polyakov gauge, the matrix  $\phi$  is given by  $\phi = \phi_3 \lambda_3 + \phi_8 \lambda_8$ . Considering that the mean field expectation values of  $\Phi$  must be real, we set  $\phi_8 = 0$  [19, 25]. The mean field traced Polyakov loop is then given by  $\Phi = \Phi^* = [1 + 2 \cos(\phi_3/T)]/3$ . Finally, the Lagrangian (1) also includes an effective potential  $\mathcal{U}$  that accounts for gauge field self-interactions and will be briefly described below.

Within this framework the mean field thermodynamical potential  $\Omega^{\text{MFA}}$  results

$$\begin{aligned} \Omega^{\text{MFA}} = -4T \sum_c \sum_n \int \frac{d^3 \vec{p}}{(2\pi)^3} \ln & \left[ \frac{(\rho_{n,\vec{p}}^c)^2 + M^2(\rho_{n,\vec{p}}^c)}{Z^2(\rho_{n,\vec{p}}^c)} \right] + \\ & + \frac{\sigma_1^2 + \kappa_p^2 \sigma_2^2}{2G_S} - \frac{\omega^2}{2G_V} + \mathcal{U}(\Phi, T), \end{aligned} \quad (4)$$

where  $M(p)$  and  $Z(p)$  are given by

$$\begin{aligned} M(p) &= Z(p) [m + \sigma_1 g(p)], \\ Z(p) &= [1 - \sigma_2 f(p)]^{-1}. \end{aligned} \quad (5)$$

Finally, as in [37], we have considered

$$(\rho_{n,\vec{p}}^c)^2 = [(2n+1)\pi T - i\mu + \phi_c]^2 + \vec{p}^2, \quad (6)$$

where  $\phi_c$  are given by the relation  $\phi = \text{diag}(\phi_r, \phi_g, \phi_b)$ . Namely,  $\phi_c = c \phi_3$  with  $c = 1, -1, 0$  for  $r, g, b$ , respectively.

For finite values of the current quark mass,  $\Omega^{\text{MFA}}$  turns out to be divergent. The regularization procedure used here considers [37, 38]

$$\Omega_{(\text{reg})}^{\text{MFA}} = \Omega^{\text{MFA}} - \Omega^{\text{free}} + \Omega_{(\text{reg})}^{\text{free}}, \quad (7)$$

where  $\Omega^{\text{free}}$  is obtained from (4) for  $\sigma_1 = \sigma_2 = 0$ , and  $\Omega_{(\text{reg})}^{\text{free}}$  is the regularized expression for the thermodynamical potential of a free fermion gas,

$$\begin{aligned} \Omega_{(\text{reg})}^{\text{free}} = -4T \frac{d^3 \vec{p}}{(2\pi)^3} \sum_c & \left[ \ln \left( 1 + \exp \left[ -\frac{\sqrt{\vec{p}^2 + m^2} - \mu + i\phi_c}{T} \right] \right) + \right. \\ & \left. + \ln \left( 1 + \exp \left[ -\frac{\sqrt{\vec{p}^2 + m^2} + \mu + i\phi_c}{T} \right] \right) \right]. \end{aligned} \quad (8)$$

---

<sup>1</sup>The corresponding values for baryon chemical potential  $\mu_B$  can easily be obtained from the relation  $\mu_B = 3\mu$ .

The next step is obtaining the mean field values of  $\sigma_1$ ,  $\sigma_2$ ,  $\omega$  and  $\Phi$  as a function of the chemical potential and the temperature, by solving the following set of coupled equations:

$$\frac{d\Omega_{(\text{reg})}^{\text{MFA}}}{d\sigma_1} = 0, \quad \frac{d\Omega_{(\text{reg})}^{\text{MFA}}}{d\sigma_2} = 0, \quad \frac{d\Omega_{(\text{reg})}^{\text{MFA}}}{d\omega} = 0, \quad \frac{d\Omega_{(\text{reg})}^{\text{MFA}}}{d\Phi} = 0. \quad (9)$$

Then we can evaluate the  $\Omega_{(\text{reg})}^{\text{MFA}}(\sigma_1, \sigma_2, \omega, \Phi, \mu, T)$  and compute all the relevant thermodynamic quantities needed in our calculation, like the chiral quark condensate

$$\langle \bar{\psi}\psi \rangle = \frac{\partial \Omega_{(\text{reg})}^{\text{MFA}}}{\partial m}, \quad \rho_q = -\frac{\partial \Omega_{(\text{reg})}^{\text{MFA}}}{\partial \mu} \quad (10)$$

and the chiral susceptibility  $\chi$  which can be used to determine the characteristic of the chiral phase transition

$$\chi_{\text{ch}} = -\frac{\partial^2 \Omega_{(\text{reg})}^{\text{MFA}}}{\partial m^2} = -\frac{\partial \langle \bar{\psi}\psi \rangle}{\partial m}. \quad (11)$$

To proceed, we still have to define some quantities like the form factors, the vector interactions, the effective potential  $\mathcal{U}$  and also the parameters of the model. Let us introduce them gradually.

**1.2. Form Factors and Wave Function Renormalization.** Following [37, 39], we have considered two different types of functional dependency for the form factors  $g(q)$  and  $f(q)$ :

exponential forms

$$(\text{Set A}) \quad \begin{cases} g(p) = \exp(-p^2/\Lambda_0^2), \\ f(p) = 0, \end{cases} \quad (12)$$

$$(\text{Set B}) \quad \begin{cases} g(p) = \exp(-p^2/\Lambda_0^2), \\ f(p) = \exp(-p^2/\Lambda_1^2), \end{cases} \quad (13)$$

and Lorentzians with WFR

$$(\text{Set C}) \quad \begin{cases} g(p) = \frac{1 + \alpha_z}{1 + \alpha_z f_z(p)} \frac{\alpha_m f_m(p) - m \alpha_z f_z(p)}{\alpha_m - m \alpha_z}, \\ f(p) = \frac{1 + \alpha_z}{1 + \alpha_z f_z(p)} f_z(p), \end{cases} \quad (14)$$

where

$$f_m(p) = \left[1 + (p^2/\Lambda_0^2)^{3/2}\right]^{-1}, \quad f_z(p) = \left[1 + (p^2/\Lambda_1^2)\right]^{-5/2}, \quad (15)$$

and  $\alpha_m = 309$  MeV,  $\alpha_z = -0.3$ . All the parameter sets are summarized in table.

Sets of parameters (see [39] for a detailed description)

Parameter	Set A	Set B	Set C
$m$ , MeV	5.78	5.7	2.37
$\Lambda_0$ , MeV	752.2	814.42	850.0
$G_S \Lambda_0^2$	20.65	32.03	20.818
$\Lambda_1$ , MeV	0.0	1034.5	1400.0
$\kappa_p$ , MeV	0.0	4180.0	6034.0

In addition, we want to include in our analysis the results arising from a local PNJL model, which allows us to compare them with the results obtained, for example, in [4]. For that purpose, we started from the Lagrangian in [21] with two flavors instead of three and we use the same model parameters as in [18, 19, 40]:

$$m = 5.5 \text{ MeV}, \quad G = 10.1 \text{ GeV}^{-2}, \quad \Lambda = 650.0 \text{ MeV}. \quad (16)$$

The model inputs can be constrained with results from lattice QCD studies. In particular, the above-described form factors of the nonlocal interaction have been chosen [39] so as to reproduce the dynamical mass function  $M(p)$  and the WFR  $Z(p)$  of the quark propagator in the vacuum [41]. In Fig. 1 we show the shapes of normalized dynamical masses and WFR for the models under discussion here, i.e., the nonlocal models with set A (rank-one), set B and set C (rank-two) parametrizations as well as the local limit.

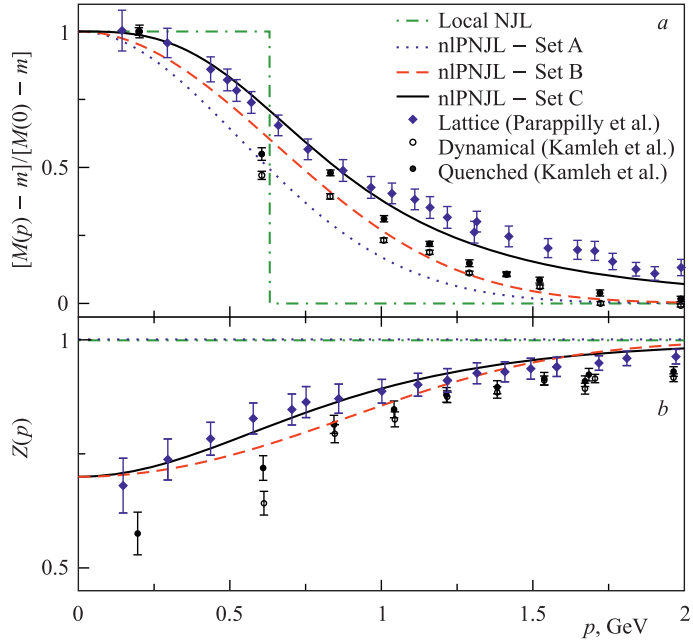


Fig. 1 (color online). Normalized dynamical masses (a) and wave function renormalization (b) for the different nonlocal form factors under study from [37, 39] fitted to lattice data from [41]. For comparison the local model [40] and more recent lattice data from [42] are also included

This figure generalizes the corresponding Fig. 1 in [39], by including the local limit for  $M(p)$  and showing the line  $Z(p) = 1$  for both, set A and the local case. For comparison, a more recent lattice data from [42] is also included. It is easy to recognize the better agreement between the lattice results and the more complete model, namely, nonlocal PNJL with WFR, in its two form factor parametrizations given by set B and set C.

**1.3. The Vector Coupling.** The vector coupling constant  $G_V$  is considered a free parameter which in the mean field approximation (MFA) may be adjusted so as to reproduce the behavior of the critical temperature,  $T_c(\mu)$ , which has recently been obtained by Taylor expansion

technique in lattice QCD [43],

$$\frac{T_c(\mu)}{T_c(0)} = 1 - \kappa \left( \frac{\mu}{T} \right)^2 + \mathcal{O} \left[ \left( \frac{\mu}{T} \right)^4 \right], \quad (17)$$

with  $\kappa = 0.059(2)(4)$  being the curvature. Note that this result is not yet based on continuum extrapolated lattice results, so that discretization errors have to be expected. However, we are interested to present here a scheme for constraining effective QCD models. The quality of predictions can subsequently be improved by using better lattice QCD data and constant discretization schemes. In what follows, the vector coupling strength will be evaluated by considering different ratios of  $\eta_V = G_V/G_S$ , and we use this parameter to tune our model to obtain better agreement with lattice predictions.

We include the vector coupling as a shifting in the chemical potential according to

$$\tilde{\mu} = \mu - \omega g(p) Z(p). \quad (18)$$

Note that we include the WFR  $Z(p)$  in the shifted chemical potential in order to keep the thermodynamical potential at mean field level. We found that the results are quite different if the  $Z(p)$  had not been included in the shift. As an example of that, we show in Fig. 2 the phase diagram for set B with and without WFR in  $\tilde{\mu}$ , for a particular value of  $\eta_V$  (similar results were obtained within set C) and a finite value of vector coupling constant.

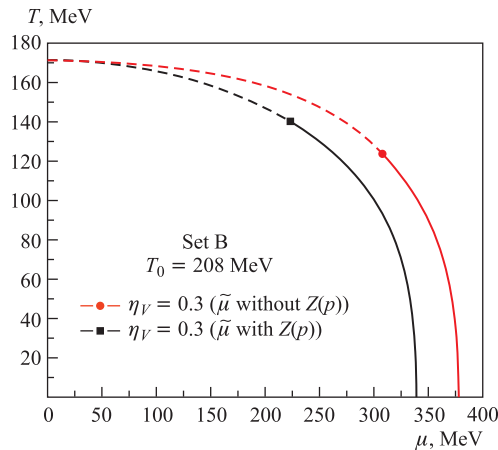


Fig. 2 (color online). Comparative plot of phase diagram obtained with and without the inclusion of  $Z(p)$  in the shifted chemical potential in Eq.(18). Dashed lines represent crossover transitions, the symbols (dot or square) indicate the critical endpoints location, and solid lines are first-order phase transitions

Finally, we have to include the shifting (18) in (6) defining a new  $\tilde{\rho}_{n,\vec{p}}^c$ .

In the case of the local model, we consider that the chemical potential is shifted by

$$\tilde{\mu} = \mu - \omega. \quad (19)$$

**1.4. Polyakov-Loop Potential.** In the present work we have chosen a  $\mu$ -dependent logarithmic effective potential described in [44]

$$\mathcal{U}(\Phi, T, \mu) = (a_0 T^4 + a_1 \mu^4 + a_2 T^2 \mu^2) \Phi^2 + a_3 T_0^4 \ln(1 - 6\Phi^2 + 8\Phi^3 - 3\Phi^4), \quad (20)$$

where

$$a_0 = -1.85, \quad a_1 = -1.44 \cdot 10^{-3}, \quad a_2 = -0.08, \quad a_3 = -0.40.$$

The reason for our particular election is that we want to consider the influence of chemical potential on the PL effective potential, and evaluate how this  $\mu$ -dependence can modify the phase diagram, tuning the vector coupling. In Fig. 3 we compare the phase diagrams we obtained considering the  $\mu$ -dependent logarithmic effective potential and a non- $\mu$ -dependent effective potential described in [19]. The results for sets A and C have a similar qualitative behavior. As expected, at  $T = 0$  and  $\mu = 0$  both potentials produce the same critical temperatures, but there is a significant difference in the location of the CEPs. Nevertheless, it is shown in the same figure that this difference turns out to be smaller when increasing the vector coupling strength.

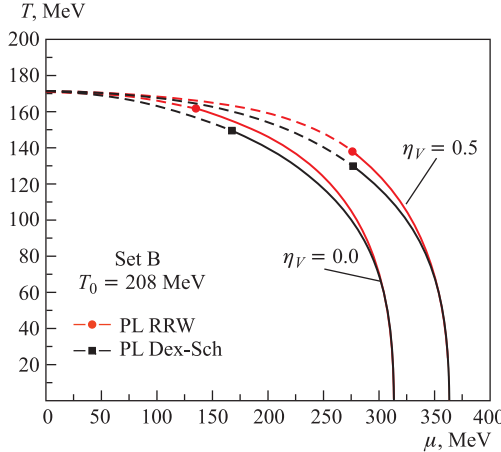


Fig. 3 (color online). Phase diagrams obtained with the  $\mu$ -dependent effective potential from [44] used in this work in comparison with the logarithmic PL potential in [19]. Dashed lines represent crossover transitions, the symbols (dots or squares) indicate the critical endpoints location, and solid lines are first-order phase transitions

Another point we have to discuss here is the election of the critical temperature  $T_0$  for deconfinement transition. In the present work we set  $T_0$  for deconfinement by using the value corresponding to two flavors, i.e.,  $T_0 = 208$  MeV, as has been suggested in [45] and used in subsequent approaches, including the nonlocal PNJL [46], Polyakov loop–DSE models [47] and entanglement PNJL (EPNJL) model [48, 49]. This election produces lower  $T_c$  values for the chiral transition (see Fig. 4 as an example), obtaining at zero chemical potential closer values to the lattice QCD more accepted result [3] for the critical temperature  $T_c(0) = 170$  MeV. It is remarkable that within the local model the obtained critical temperatures are noticeably higher than in the case of nonlocal models, as is shown in Fig. 4.

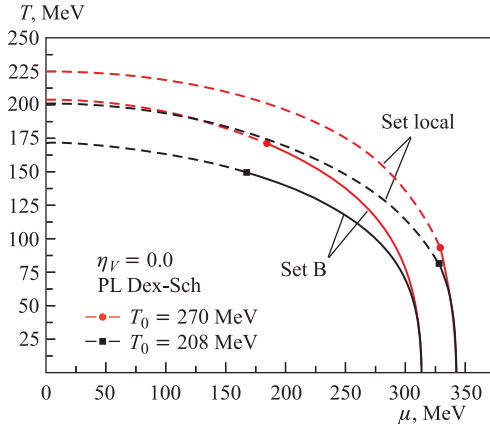


Fig. 4 (color online). Comparison of phase diagrams determined with two different values of the deconfinement critical temperature  $T_0$ : the pure gauge value ( $T_0 = 270$  MeV) and the two-flavor value ( $T_0 = 208$  MeV). See [45–47] for details. Dashed lines represent crossover transitions, the symbols (dots or squares) indicate the critical endpoints location, and solid lines are first-order phase transitions

In this context it is important to keep in mind the effect that the account for a hadronic phase can have on the topology of the QCD phase diagram [50, 51], as well as higher-order quark interactions [52].

## 2. RESULTS

The first effect we want to study is how the vector interactions affect the transitions and the location of the CEP. We built the corresponding phase diagrams for different values of  $\eta_V$ . In all the cases we observed a variation in the curvatures even at low chemical potential. As expected, the influence of the vector coupling increases with the chemical potential, then the position of the CEP and the values of  $\mu_c(T = 0)$  reflect notably this influence. We want to remark that, for increasing  $\eta_V$ , the CEPs tend to be located towards lower  $T$  and higher  $\mu$ . Similarly to what has been shown in [53], we observe that for any of the nonlocal models under study, the CEPs (and the corresponding first-order transitions) are still present for all the values of vector coupling constant analyzed in this work. In Fig. 5 it can be seen that effect for set B (qualitatively similar behavior was observed for set A and set C). Nevertheless, for the local model, we observe that by increasing  $\eta_V$  a crossover line without a CEP is obtained, as is shown in Fig. 6.

Once we have the phase diagrams, the next step is to determine the curvatures. To do so, we plotted the pseudocritical temperatures of the crossover transitions as a function of  $(\mu/T)^2$  for different  $\eta_V$  ratios. Then, the curvatures can be obtained from the slope of the straight lines in the region of low  $(\mu/T)$  values. An example of this is shown in Fig. 7 for set C (the corresponding plots for the other sets are qualitatively very similar). The fit of the lattice QCD results (17) is also shown. The grey zone corresponds to the error in the coefficient  $\kappa$  obtained in [43].

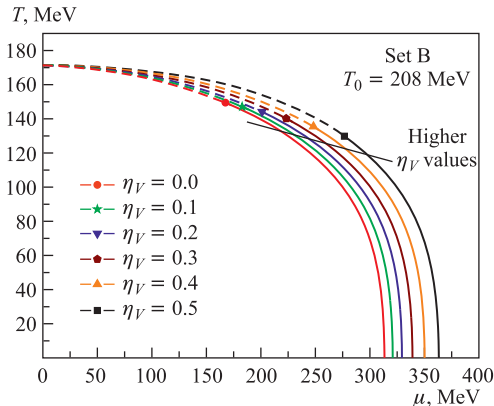


Fig. 5 (color online). Influence of the strength of the vector coupling (here  $\eta_V = G_V/G_S$ ) on the phase diagram for set B. Dashed lines represent crossover transitions, the symbols indicate the critical endpoints locations, and solid lines are first-order phase transitions

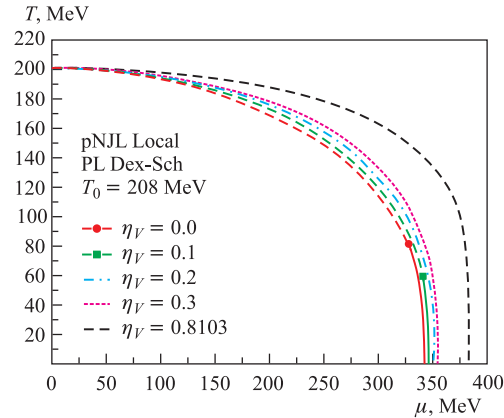


Fig. 6 (color online). Influence of the strength of the vector coupling on the phase diagram for the local model. Dashed lines represent crossover transitions, the symbols (dot or square) indicate the critical endpoints location, and solid lines are first-order phase transitions. It can be seen that CEPs tend to disappear for  $G_V > 0.1G_S$ , leaving only a crossover phase transition

In Fig. 8 we compare the lattice result with the values for the coefficient  $\kappa$  obtained within the nonlocal PNJL models and the local one. There, the horizontal line corresponds to the lattice QCD prediction of  $\kappa = 0.059(2)(4)$  [43] and the grey zone represents its error. Note

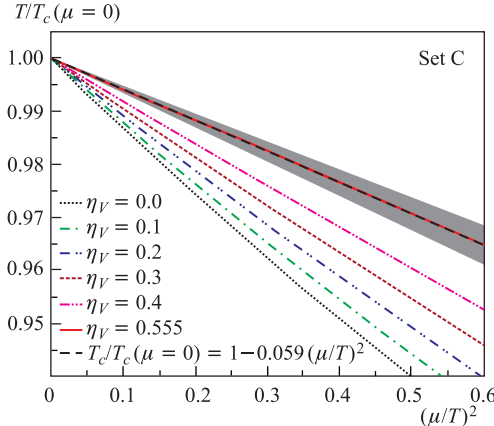


Fig. 7 (color online). Chiral crossover transitions at low values of  $\mu/T$  for different values of strengths of the vector coupling  $\eta_V = G_V/G_S$  for set C. The dashed line corresponds to the lattice QCD prediction of  $\kappa = 0.059(2)(4)$  [43]

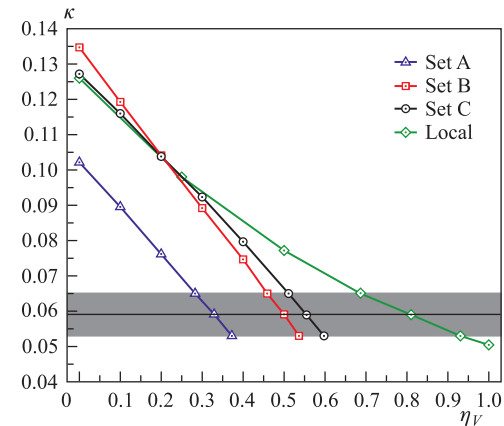


Fig. 8 (color online). Curvature  $\kappa$  of the pseudo-critical temperature  $T_c(\mu)$  of the chiral crossover transition at low values of  $\mu/T$ . The horizontal line corresponds to the lattice QCD prediction of  $\kappa = 0.059(2)(4)$  [43]. The grey zone represents the corresponding error in the curvature determination

that for the more complete model (set B and set C) the curvatures are closer to each other than in the case of set A and local ones.

It is important to remark that while the analysis of  $\kappa$  has been performed for  $N_f = 2 + 1$  simulations, the chemical potential  $\mu$  concerns only the two light flavors. Therefore, our extraction of  $\kappa$  from the nonlocal PNJL models for the 2-flavor case may be in order.

In Fig. 9 the phase diagrams for the nonlocal models discussed in this work are compared, considering the corresponding  $\eta_V$  values that best fit the lattice QCD prediction of  $\kappa = 0.059(2)(4)$  from [43]. The grey zones correspond to the range of  $\eta_V$  values obtained by considering the error in the lattice determination of  $\kappa$  [43]. Similarly, the error bars in the CEPs indicate the distances to the CEP positions for the corresponding  $\eta_V$  values that fit the error limits.

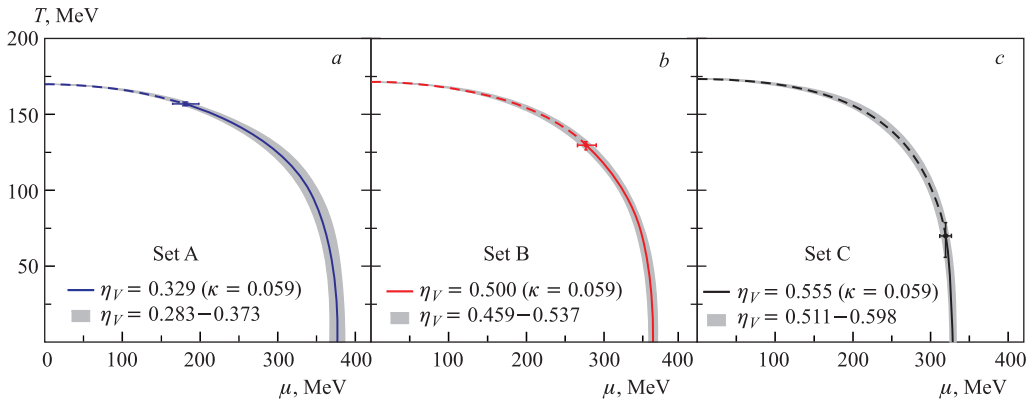


Fig. 9 (color online). Phase diagrams obtained with the nonlocal models with the parametrizations set A (a), set B (b) and set C (c), for the values of  $\eta_V$  that best fit the lattice QCD prediction in [43]. The grey zones and the error bars of the CEP location represent the corresponding indetermination for the curvature value

Note that by using the Polyakov loop potential (20) from [44], a crossover region and a CEP can be obtained for set A, even for  $T_0 = 208$  MeV, contrarily to what has been reported in [46, 47], where the Polyakov loop potential from [19] has been used.<sup>1</sup>

The results summarized in Fig. 10 indicate that the absolute value of the critical temperature  $T_c(0)$  of nonlocal covariant PNJL models is rather insensitive to the choice of the form factors parametrizing the momentum dependence of dynamical (running) mass function and WFR of the quark propagator as measured on the lattice at zero temperature [41], whereas the position of the CEP and critical chemical potential at  $T = 0$  strongly depends on it. On the other hand, the value of  $T_c(0)$  in the local model is significantly different (larger) than in the nonlocal ones. In addition, note that in the local model to fit the lattice QCD value requires a larger vector coupling, for which the corresponding phase diagram lacks of CEP and all the chiral phase transition is a crossover. This is another remarkable difference with respect to the phase diagram obtained with nonlocal models [4].

---

<sup>1</sup>Note that in the low- $\mu$  region the differences in the chiral transition obtained with each effective potential are mainly due to the definition of the corresponding logarithmic term in the Polyakov-loop potential.

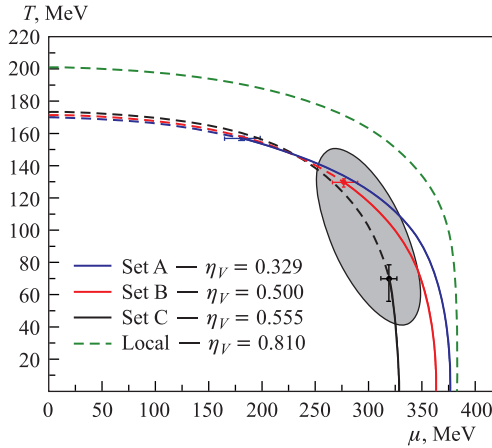


Fig. 10 (color online). Phase diagrams with (pseudo)critical temperatures  $T_c(\mu)$  and critical points for nonlocal PNJL models (sets A–C) compared to the local one. Dashed (full) lines correspond to crossover (first-order) transitions. The vector coupling strength  $\eta_V$  is chosen so that these models reproduce the lattice QCD result  $\kappa = 0.059(2)(4)$  [43] for the curvature at low  $\mu$  values. The corresponding values for  $T_c(\mu = 0)$  (in MeV) are 169.9, 171.3, 173.2 and 200.9, for sets A, B, C and local, respectively. The highlighted region denotes the CEP position favored by the present study

The nonlocal model for the set B and set C cases contains WFR and dynamical (running) quark mass effects, and thus is closer to full QCD. Therefore, we suggest that statements about the existence and location of the CEP within set A and the local model should be less trustworthy than those of set B and set C. As a consequence, a possible region for the CEP location suggested by our study would be between the results for set B and set C, i.e., around  $(T_{\text{CEP}}, \mu_{\text{CEP}}) = (129.8, 276.6$  MeV) and  $(69.9, 319.1$  MeV), respectively.

This suggests that the search for CEP signatures in the BES programs is justified and should be continued. The energy range of the NICA and FAIR facilities shall be particularly promising.

### 3. SUMMARY AND CONCLUSIONS

In this work, based on nonlocal PNJL models with and without WFR, we have studied the influence of vector coupling strength in the QCD phase diagram. As shown in Fig. 2, a remarkable difference is observed when the shift of the chemical potential includes the WFR function, keeping the thermodynamical potential at mean field level. In a further exploratory step, we showed the influence of considering different values for the  $T_0$  parameter in the effective potential on the phase diagrams (see Fig. 4). As expected, a noticeable decrease of the chiral transition critical temperatures is observed, but the smaller the temperature, the smaller is this decrease, converging to almost the same value when the critical temperature goes below  $T = 40$  MeV. Also in Fig. 4, one can see from a comparison between one of the nonlocal models (set B as an example) and the local one that a remarkable difference of about 25 MeV along all the phase diagram lines for the same value of  $T_0$  is obtained. But the main variation is in the location of the CEP, which in

the case of the local model turns out to be at a lower  $T$  and higher  $\mu$  than in the nonlocal case. Comparing Figs. 5 and 6 for nonlocal and local models, respectively, it can be observed that the influence of the increasing of the vector coupling strength is qualitatively similar in both cases, i.e., moving the phase transitions towards higher  $\mu$  values and lowering the CEP location. Nevertheless, in the case of the local model the CEP turns out to disappear for higher values of  $\eta_V$ , leaving only a crossover transition along all the phase diagrams.

A second step in our work consisted in the determination of the curvatures in the low  $\mu$  region as the slope of the straight lines obtained by plotting the pseudocritical temperatures of the crossover transitions as a function of  $(\mu/T)^2$ . In Fig. 7 are shown some examples of the lines obtained with set C and several values of  $\eta_V$ , while in Fig. 8 it can be observed how the curvatures vary with respect to the vector coupling strength for all the parametrizations considered.

Once the values of  $\eta_V$  have been determined that best reproduce the lattice QCD result  $\kappa = 0.059(2)(4)$  [43] for the curvature at low  $\mu$  values, we have shown (Fig. 9) the nonlocal model phase diagrams for the obtained values of  $\eta_V$ .

Finally, considering the more elaborated models (nonlocal and with WFR, i.e., set B and set C), and the corresponding values of  $\eta_V$  adjusted to lattice QCD results, we suggest in Fig. 10 the most likely zone where, according to our study, the CEP would be located.

Note that in this exploratory study the lattice QCD data for the quark propagator and for the curvature of the pseudocritical line are obtained with different lattice actions. A more consistent study should be based on the same discretization of the action, provide a continuum extrapolation and work with physical quark masses.

As a next step, it is necessary to investigate the robustness of the results of the non-local PNJL models when modifying the choice of the Polyakov-loop potential taking into account recent developments [54–56] and, in particular, when going beyond the mean field approximation. A scheme for going beyond the mean field in nonlocal PNJL models by including hadronic correlations (bound states and their dissociation in the continuum of scattering states) has recently been developed [57] and shall be generalized for studies of the chiral and deconfinement phase transition in the QCD phase diagram. A key quantity for such studies will be the hadronic spectral function. First results using a generic ansatz [58] for joining the hadron resonance gas and PNJL approaches are promising [59, 60] and have recently been underpinned a microscopic justification by a treatment of pion dissociation within the (local) PNJL model [61]. This approach has recently been generalized by mimicking confining properties with an infrared momentum cutoff [62] in order to bind higher lying mesonic states such as the sigma meson — a feature shared with the nonlocal extensions of the (P)NJL model as, e.g., in [23, 47, 63, 64], to be exploited further in subsequent work.

**Acknowledgements.** We would like to thank O. Kaczmarek, S. Nedelko, K. Redlich, C. Schmidt, and N. Scoccolla for useful comments and discussions. D.B. acknowledges hospitality and support during his visit at the University of Bielefeld and funding of his research provided by the Polish Narodowe Centrum Nauki within the «Maestro» programme under contract UMO-2011/02/A/ST2/00306, as well as by the Russian Foundation for Basic Research under Grant No. 11-02-01538-a. G.C. is grateful for support by CONICET (Argentina) and by «CompStar», a research networking programme of the European Science Foundation.

## REFERENCES

1. Stephanov M.A. QCD Phase Diagram: An Overview // PoS LAT 2006. 2006. 024.
2. Bazavov A. et al. The Chiral and Deconfinement Aspects of the QCD Transition // Phys. Rev. D. 2012. V. 85. P. 054503.
3. Ejiri S. Lattice QCD at Finite Temperature // Nucl. Phys. Proc. Suppl. 2001. V. 94. P. 19.
4. Bratovic N.M., Hatsuda T., Weise W. Role of Vector Interaction and Axial Anomaly in the PNJL Modeling of the QCD Phase Diagram // Phys. Lett. B. 2013. V. 719. P. 131.
5. Carignano S., Nickel D., Buballa M. Influence of Vector Interaction and Polyakov Loop Dynamics on Inhomogeneous Chiral Symmetry Breaking Phases // Phys. Rev. D. 2010. V. 82. P. 054009.
6. Kitazawa M. et al. Chiral and Color Superconducting Phase Transitions with Vector Interaction in a Simple Model // Prog. Theor. Phys. 2002. V. 108. P. 929.
7. Blaschke D., Volkov M.K., Yudichev V.L. Coexistence of Color Superconductivity and Chiral Symmetry Breaking within the NJL Model // Eur. Phys. J. A. 2003. V. 17. P. 103.
8. Hatsuda T. et al. New Critical Point Induced by the Axial Anomaly in Dense QCD // Phys. Rev. Lett. 2006. V. 97. P. 122001.
9. Bowman E.S., Kapusta J.I. Critical Points in the Linear Sigma Model with Quarks // Phys. Rev. C. 2009. V. 79. P. 015202.
10. Kunihiro T., Minami Y., Zhang Z. QCD Critical Points and Their Associated Soft Modes // Prog. Theor. Phys. Suppl. 2010. V. 186. P. 447.
11. Zhang Z., Kunihiro T. Vector Interaction, Charge Neutrality and Multiple Chiral Critical Point Structures // Phys. Rev. D. 2009. V. 80. P. 014015.
12. Blaschke D. et al. Exploring the QCD Phase Diagram with Compact Stars // Nucl. Phys. Proc. Suppl. 2005. V. 141. P. 137.
13. Andronic A. et al. Hadron Production in Ultra-relativistic Nuclear Collisions: Quarkyonic Matter and a Triple Point in the Phase Diagram of QCD // Nucl. Phys. A. 2010. V. 837. P. 65.
14. Nambu Y., Jona-Lasinio G. Dynamical Model of Elementary Particles Based on an Analogy with Superconductivity // Phys. Rev. 1961. V. 122. P. 345; V. 124. P. 246.
15. Vogl U., Weise W. The Nambu and Jona-Lasinio Model: Its Implications for Hadrons and Nuclei // Prog. Part. Nucl. Phys. 1991. V. 27. P. 195.
16. Klevansky S.P. The Nambu–Jona-Lasinio Model of Quantum Chromodynamics // Rev. Mod. Phys. 1992. V. 64. P. 649.
17. Hatsuda T., Kunihiro T. QCD Phenomenology Based on a Chiral Effective Lagrangian // Phys. Rep. 1994. V. 247. P. 221.
18. Ratti C., Thaler M.A., Weise W. Phases of QCD: Lattice Thermodynamics and a Field Theoretical Model // Phys. Rev. D. 2006. V. 73. P. 014019.
19. Roessner S., Ratti C., Weise W. Polyakov Loop, Diquarks and the Two-Flavour Phase Diagram // Phys. Rev. D. 2007. V. 75. P. 034007.
20. Sasaki C., Friman B., Redlich K. Susceptibilities and the Phase Structure of a Chiral Model with Polyakov Loops // Ibid. P. 074013.
21. Fukushima K. Phase Diagrams in the Three-Flavor Nambu–Jona-Lasinio Model with the Polyakov Loop // Phys. Rev. D. 2008. V. 77. P. 114028; Erratum // Ibid. V. 78. P. 039902.
22. Abuki H. et al. Chiral Crossover, Deconfinement and Quarkyonic Matter within a Nambu–Jona-Lasinio Model with the Polyakov Loop // Ibid. P. 034034.
23. Schmidt S.M., Blaschke D., Kalinovsky Y.L. Scalar-Pseudoscalar Meson Masses in Nonlocal Effective QCD at Finite Temperature // Phys. Rev. C. 1994. V. 50. P. 435.

24. *Efimov G. V., Nedelko S. N.* Nambu–Jona-Lasinio Model with the Homogeneous Background Gluon Field // Phys. Rev. D. 1995. V. 51. P. 176.
25. *Contrera G. A., Gomez Dumm D., Scoccola N. N.* Nonlocal  $SU(3)$  Chiral Quark Models at Finite Temperature: The Role of the Polyakov Loop // Phys. Lett. B. 2008. V. 661. P. 113.
26. *Demorest P. et al.* Shapiro Delay Measurement of a Two Solar Mass Neutron Star // Nature. 2010. V. 467. P. 1081.
27. *Antoniadis J. et al.* A Massive Pulsar in a Compact Relativistic Binary // Science. 2013. V. 340. P. 6131.
28. *Klähn T. et al.* Modern Compact Star Observations and the Quark Matter Equation of State // Phys. Lett. B. 2007. V. 654. P. 170.
29. *Orsaria M. et al.* Quark-Hybrid Matter in the Cores of Massive Neutron Stars // Phys. Rev. D. 2013. V. 87. P. 023001.
30. *Klähn T., Blaschke D. B., Lastowiecki R.* Implications of the Measurement of Pulsars with Two Solar Masses for Quark Matter in Compact Stars and HIC. A NJL Model Case Study // Ibid. V. 88. P. 085001.
31. *Orsaria M. et al.* Quark Deconfinement in High-Mass Neutron Stars. arXiv:1308.1657 [nucl-th].
32. *Shao G. Y. et al.* Isoscalar-Vector Interaction and Hybrid Quark Core in Massive Neutron Stars. arXiv:1305.1176 [nucl-th].
33. *Blaschke D. B. et al.* Hybrid Stars within a Covariant, Nonlocal Chiral Quark Model // Phys. Rev. C. 2007. V. 75. P. 065804.
34. *Blaschke D. et al.* Nonlocal PNJL Models and Heavy Hybrid Stars // PoS Confinement X. 2012. 249.
35. *Blaschke D., Alvarez-Castillo D. E., Benic S.* Mass-Radius Constraints for Compact Stars and a Critical Endpoint // PoS CPOD 2013. 2013. 063; arXiv:1310.3803 [nucl-th].
36. *Alvarez-Castillo D. E. et al.* Crossover Transition to Quark Matter in Heavy Hybrid Stars. arXiv:1311.5112 [nucl-th].
37. *Contrera G. A., Orsaria M., Scoccola N. N.* Nonlocal Polyakov–Nambu–Jona-Lasinio Model with Wave Function Renormalization at Finite Temperature and Chemical Potential // Phys. Rev. D. 2010. V. 82. P. 054026.
38. *Gomez Dumm D., Scoccola N. N.* Characteristics of the Chiral Phase Transition in Nonlocal Quark Models // Phys. Rev. C. 2005. V. 72. P. 014909.
39. *Noguera S., Scoccola N. N.* Nonlocal Chiral Quark Models with Wavefunction Renormalization: Sigma Properties and Pion–Pion Scattering Parameters // Phys. Rev. D. 2008. V. 78. P. 114002.
40. *Gomez Dumm D. et al.* Color Neutrality Effects in the Phase Diagram of the PNJL Model // Ibid. P. 114021.
41. *Parappilly M. B. et al.* Scaling Behavior of Quark Propagator in Full QCD // Phys. Rev. D. 2006. V. 73. P. 054504.
42. *Kamleh W. et al.* Unquenching Effects in the Quark and Gluon Propagator // Phys. Rev. D. 2007. V. 76. P. 094501.
43. *Kaczmarek O. et al.* Phase Boundary for the Chiral Transition in  $(2 + 1)$ -Flavor QCD at Small Values of the Chemical Potential // Phys. Rev. D. 2011. V. 83. P. 014504.
44. *Dexheimer V. A., Schramm S.* A Novel Approach to Model Hybrid Stars // Phys. Rev. C. 2010. V. 81. P. 045201.
45. *Schaefer B.-J., Pawłowski J. M., Wambach J.* The Phase Structure of the Polyakov Quark–Meson Model // Phys. Rev. D. 2007. V. 76. P. 074023.

46. *Pagura V., Gómez Dumm D., Scoccola N.N.* Deconfinement and Chiral Restoration in Non-Local PNJL Models at Zero and Imaginary Chemical Potential // *Phys. Lett. B.* 2012. V. 707. P. 76.
47. *Horvatic D. et al.* Width of the QCD Transition in a Polyakov-Loop DSE Model // *Phys. Rev. D.* 2011. V. 84. P. 016005.
48. *Sakai Y. et al.* Entanglement between Deconfinement Transition and Chiral Symmetry Restoration // *Phys. Rev. D.* 2010. V. 82. P. 076003.
49. *Dutra M. et al.* Polyakov–Nambu–Jona-Lasinio Phase Diagrams and Quarkyonic Phase from Order Parameters // *Phys. Rev. D.* 2013. V. 88. P. 114013.
50. *Blaschke D.B. et al.* Accessibility of Color Superconducting Quark Matter Phases in Heavy-Ion Collisions // *Acta Phys. Polon. Suppl.* 2010. V. 3. P. 741.
51. *Shao G. Y. et al.* Phase Diagrams in the Hadron-PNJL Model // *Phys. Rev. D.* 2011. V. 84. P. 034028.
52. *Sasaki T. et al.* QCD Phase Diagram at Finite Baryon and Isospin Chemical Potentials // *Phys. Rev. D.* 2010. V. 82. P. 116004.
53. *Hell T., Kashiwa K., Weise W.* Impact of Vector-Current Interactions on the QCD Phase Diagram // *J. Mod. Phys.* 2013. V. 4. P. 644.
54. *Sasaki C., Redlich K.* An Effective Gluon Potential and Hybrid Approach to Yang–Mills Thermodynamics // *Phys. Rev. D.* 2012. V. 86. P. 014007.
55. *Ruggieri M. et al.* Polyakov Loop and Gluon Quasiparticles in Yang–Mills Thermodynamics // *Ibid.* P. 054007.
56. *Fukushima K., Kashiwa K.* Polyakov Loop and QCD Thermodynamics from the Gluon and Ghost Propagators // *Phys. Lett. B.* 2013. V. 723. P. 360.
57. *Radzhabov A. E. et al.* Nonlocal PNJL Model beyond Mean Field and the QCD Phase Transition // *Phys. Rev. D.* 2011. V. 83. P. 116004.
58. *Blaschke D. B. et al.* Chiral Condensate and Chemical Freeze-Out // *Phys. Part. Nucl. Lett.* 2011. V. 8. P. 811; *Few Body Syst.* 2012. V. 53. P. 99.
59. *Turko L. et al.* Mott–Hagedorn Resonance Gas and Lattice QCD Results // *Acta Phys. Polon. Suppl.* 2012. V. 5. P. 485.
60. *Turko L. et al.* An Effective Model of QCD Thermodynamics // *J. Phys. Conf. Ser.* 2013. V. 455. P. 012056.
61. *Wergieluk A. et al.* Pion Dissociation and Levinson’s Theorem in Hot PNJL Quark Matter // *Phys. Part. Nucl. Lett.* 2013. V. 10. P. 660.
62. *Dubinin A., Blaschke D., Kalinovsky Y. L.* Pion and Sigma Meson Dissociation in a Modified NJL Model at Finite Temperature. arXiv:1312.0559 [hep-ph].
63. *Benic S., Blaschke D.* Finite Temperature Mott Transition in a Nonlocal PNJL Model // *Acta Phys. Polon. Suppl.* 2013. V. 6. P. 947.
64. *Benic S. et al.* Medium Induced Lorentz Symmetry Breaking Effects in Nonlocal PNJL Models // *Phys. Rev. D.* 2013. V. 88 (in press); arXiv:1306.0588 [hep-ph].

Received on December 20, 2013.